

Cluster formation during particle settling in stratified fluid

David Deepwell¹ and Bruce R. Sutherland ^{1,2,*}

¹*Department of Physics, University of Alberta, Edmonton, Alberta T6G 2E1, Canada*

²*Department of Earth & Atmospheric Sciences,
University of Alberta, Edmonton, Alberta T6G 2E3, Canada*



(Received 15 August 2021; accepted 23 December 2021; published 5 January 2022)

To gain insight into the microscopic processes leading to the observed collective settling of particles from the base of a particle-bearing fresh water layer overlying salt water, we perform numerical simulations of the settling of weakly inertial particles through uniform density, uniformly stratified and nonuniformly stratified fluids. Intuition is gained first through simulations of a descending horizontal row and planar arrays of particles. These show that stratification acts to reduce cluster sizes and to slow the relative descent speed of clusters as a result of upward flows that develop around the clusters. This occurs even for a descending vertical planar array: in unstratified fluid, the ambient fluid rises laterally around the particles with the flow in the plane of the particles being predominantly downward; in stratified fluid, upward as well as downward motion is evident in the plane of particles. For a random three-dimensional particle array with concentration by volume between 0.1% and 1%, upflows in the ambient fluid likewise retard cluster formation and descent speeds. The mean horizontal displacement of the particles is reduced, resulting in more small clusters with more closely packed particles. The particles become more vertically aligned in lower diffusivity (higher Schmidt number) fluid, although such clustering takes longer to develop. The results suggest that both stratification and relative diffusivity play a crucial role in the collective settling behavior observed in laboratory experiments.

DOI: [10.1103/PhysRevFluids.7.014302](https://doi.org/10.1103/PhysRevFluids.7.014302)

I. INTRODUCTION

Accurate modeling of particle settling rates is important for several industrial problems (e.g., tailing ponds and waste water treatment plants [1]) and in natural environmental processes (e.g., descending ash from volcanic eruptions [2,3] and the influence upon the marine carbon pump of sinking deceased diatoms after an algal bloom [4]). Of particular interest, which ultimately motivated the present study, is the transport and deposition of clay, silt, and possibly microplastics by a muddy river entering the ocean [5]. In most circumstances the concentration of relatively dense particles is so small that the particle-bearing river plume is buoyant with respect to the saline ocean and so forms a hypopycnal current, which intrudes along the ocean surface. From this overlying flow, suspended dense particles gradually rain out of the current, eventually settling onto the ocean floor. Correct predictions of the transport and settling behavior is key to predicting where sediments and microplastics are ultimately deposited.

While descending below the river plume, the settling speed of particles can be reduced in regions of strong stratification resulting in the particles accumulating at higher concentrations [6,7]. If the concentrations become sufficiently high, then the particles may interact, possibly clustering to form effectively larger particles that collectively fall at faster speeds than that of an individual particle.

*bruce.sutherland@ualberta.ca; <https://sites.ualberta.ca/~bsuther>

Indeed, it is observed that collective settling speeds may be orders of magnitude faster [8–10]. These dynamics are readily apparent in laboratory experiments in which a layer of fresh water mixed with dense particles overlies a stationary saline ambient fluid [11–14]. Very fine particles slowly settled within the fresh water, accumulating at the interface between the fresh and salt water. Thereafter, particles were observed to descend not as a uniform cloud, but in individual, small-scale fingers and so-called “leaky ducts” [11]. This organization of particles resulting in rapid collective settling has been attributed to double-diffusive fingering and Rayleigh-Taylor (convective) instability [13,15,16]. In developing these models for instability the suspended particles were treated as a continuous scalar field. This is valid when the particles are small with negligible inertia, and having low concentration. However, as will be reviewed below, it is known that weakly inertial particles in stratified fluid can be drawn together. Consequently, such microscopic dynamics may act to influence the macroscopic formation, for example, of leaky ducts as the particles pass through the relatively thick interface separating particle-bearing fresh water and the underlying saline ambient fluid.

As a step toward gaining insight into the microscopic dynamics involved with the settling of weakly inertial particles, here we perform particle-resolving numerical simulations to examine particle interactions, clustering, and enhanced/hindered settling in a Boussinesq fluid. Our focus is upon particle settling in uniform stratification in contrast with settling in uniform density fluid. However, we also consider settling from a uniformly stratified layer overlying a uniform density fluid.

There have been several experimental and numerical studies that focused on the settling of an individual weakly inertial particle passing through either a sharp density interface [17–21] or descending in uniform stratification [22,23]. These studies showed that the particle decelerated not just because the background density increased with depth (so reducing the negative buoyancy of the particle with respect to its surroundings) but also because the particle carried less-dense fluid in its wake. Hence, not only did stratification influence the particle, but the particle adjusted the stratification through either mixing or transport of density and possibly biogeochemical components [23].

Even in uniform density fluid, the settling of a pair of particles can be quite complex, depending upon their relative size and density [24–26]. In particular, for two equal-sized noninertial spherical particles, Kynch [24] predicted that the pair settles only in the vertical if they are vertically or horizontally aligned. Otherwise, the pair drifts laterally as they descend. These dynamics were likewise observed for a particle pair crossing a density interface [27]. In uniform stratification a vertically aligned pair approach each other and then separate; horizontally aligned particles move toward each other [28].

A handful of theoretical-numerical studies exist examining the settling of more than two particles, though most of these have assumed a uniform density ambient fluid. Although stable configurations exist for up to six particles situated at the vertices of a regular polygon [29,30], in most cases the relative orientation of the particles change as they descend. Ganatos *et al.* [31] showed that the settling of three particles typically form into a leading pair and a trailing orphan. In a theoretical-experimental examination of a one-dimensional horizontal row of equally spaced particles initialized at rest, Crowley [32] demonstrated that the settling particles form clusters through an instability caused by viscous fluid forces. The fastest growing mode consisted of four particles in which one particle was slightly below the others and acted as an attractor for the nearest neighbors. Gradually this instability grew into a cluster of three particles settling faster than the one left behind. This form of clustering was consistent over the entire row. He went on to extend this work to a horizontal planar array of particles, demonstrating that the interaction between all particles, not just nearest neighbors, must be accounted for when a sizable distribution of particles are present [33,34].

Building upon the foundation of Crowley and others, here we include the influence of stratification to investigate the sedimentation sequentially of a row, a plane, and a three-dimensional distribution of particles to examine the particle interactions at these increasing levels of complexity. Section II describes the numerical formulation and model. We go on to present in Sec. III the settling of a row of particles, in Sec. IV the settling of a two-dimensional horizontal and vertical plane of

particles, and in Sec. V the settling of a three-dimensional suspension. Discussion and conclusions are given in Sec. VI.

II. METHODS

So as to evaluate the microdynamics of the interactions between particles and between the particles and background stratification, numerical simulations were performed to examine the sedimentation of initially stationary monodisperse, spherical particles in a uniformly and nonuniformly stratified fluid. We used the numerical model developed by Eckart Meiburg's group at UC Santa Barbara using the Immersed Boundary Method (IBM) [35]. This code has been used to simulate the consolidation of settling sediment [36], interfacial mixing due to migrating swimmers [37], and the settling of a particle pair through a sharp interface [27]. Model validation was demonstrated by these authors through comparison of model results to laboratory measurements of the settling of an individual particle.

A. Governing equations

A stratified, Boussinesq, incompressible fluid is governed by the following equations:

$$\frac{D\mathbf{u}}{Dt} = -\frac{1}{\rho_0}\nabla p + \frac{\rho}{\rho_0}\mathbf{g} + \nu\nabla^2\mathbf{u} + \mathbf{f}_{\text{IBM}}, \quad (1a)$$

$$\nabla \cdot \mathbf{u} = 0, \quad (1b)$$

$$\frac{D\rho}{Dt} = \kappa\nabla^2\rho, \quad (1c)$$

where $\mathbf{u} = (u, v, w)$ is the velocity vector with w being the vertical velocity, p is the total pressure, ρ is the local fluid density, ρ_0 is a reference density (the background density at depth $z = 0$), $\mathbf{g} = -g\mathbf{k}$ is gravity acting opposite to the upward vertical direction \mathbf{k} , ν is the kinematic viscosity, κ is the diffusivity of the fluid, and \mathbf{f}_{IBM} are the forces caused by the particles [35,38].

The motion of an individual particle of density, ρ_p , and diameter, D_p , is governed by

$$m_p \frac{d\mathbf{u}_p}{dt} = \oint_{\Gamma_p} \mathcal{T} \cdot \mathbf{n} dA + V_p(\rho_p - \rho_0)g\mathbf{k} + \mathbf{F}_c, \quad (2a)$$

$$I_p \frac{d\boldsymbol{\omega}_p}{dt} = \oint_{\Gamma_p} \mathbf{r} \times (\mathcal{T} \cdot \mathbf{n}) dA + \mathbf{T}_c, \quad (2b)$$

in which $\mathcal{T} \equiv -p\mathbf{I} + \rho_0\nu[\nabla\mathbf{u} + (\nabla\mathbf{u})^T]/2$ is the hydrodynamic stress tensor, V_p is the volume of the particle, $m_p = V_p\rho_p$ is its mass, $I_p = \pi\rho_p D_p^5/60$ is its moment of inertia, and \mathbf{r} is the radial vector from the center of the particle. The outward pointing normal of the surface, Γ_p , of each particle is \mathbf{n} . The forces and torques arising due to particle collisions are denoted by \mathbf{F}_c and \mathbf{T}_c . These involve models accounting for lubrication forces as well as normal contact and tangential collisions, as described in Biegert *et al.* [35]. In addition to the collision forces, the IBM method directly couples the fluid and particle phases through the stress tensor, \mathcal{T} .

The natural explicit length and velocity scales of the problem, respectively, are the particle diameter, D_p , and the Stokes settling velocity for noninertial particles, w_s :

$$w_s = \frac{1}{18} \frac{\rho_p - \rho_0}{\rho_0} \frac{gD_p^2}{\nu}. \quad (3)$$

The corresponding characteristic timescale is $\tau = D_p/w_s$. In addition, the strength of the background stratification is given in terms of the buoyancy frequency, $N = \sqrt{g\gamma/\rho_0}$, in which γ is the magnitude of the background density gradient (taken to be the largest value in nonuniformly

stratified fluid). Using these scales, the importance of stratification, viscosity and relative diffusivity are expressed, respectively, in terms of the following nondimensional numbers:

$$\text{Fr} = \frac{w_s}{ND_p} \quad \text{Froude Number}, \quad (4a)$$

$$\text{Re} = \frac{w_s D_p}{\nu} \quad \text{Reynolds Number}, \quad (4b)$$

$$\text{Pe} = \text{ScRe} = \frac{w_s D_p}{\kappa} \quad \text{Péclet Number}, \quad (4c)$$

in which $\text{Sc} = \nu/\kappa$ is the Schmidt number.

The settling of small suspended particles in marine coastal environments is typically slow, with Reynolds numbers ranging from 1 for fine sand to 7×10^{-6} for clay. In most cases, we suppose the particles are weakly inertial by setting the Reynolds number to be $1/4$. This relatively large value is chosen to reduce computational cost. However, as we show in Appendix B, the value is sufficiently small to capture the particle-interaction dynamics of even smaller (lower Reynolds number) particles.

Using a particle of diameter of $80 \mu\text{m}$, a particle Reynolds number of $1/4$, and the viscosity of water, Eq. (3) gives the relative particle density to be $\rho_p/\rho_0 \simeq 1.9$, which is comparable to that of clays, sand and the silicon carbide, silica and glass microsphere particles used in laboratory experiments [11,13,14]. In Appendix B, different particle densities are used in studies of the influence of the Reynolds number upon particle settling.

Also to reduce computational cost, in most simulations a constant Schmidt number of $\text{Sc} = 7$ was used. Though much smaller than values characteristic of the ratio of viscosity to salinity diffusion in water, it is a suitable choice for thermally stratified fluids. That said, because this work is motivated by laboratory experiments using salt-stratified fluid, a limited number of simulations were performed with $\text{Sc} = 70$ to examine the influence of lower diffusivity on particle settling and clustering. Lower diffusivity is known to have a nonnegligible influence on single-particle settling through the development of a vertically asymmetric wake in strong stratification [39]. Its influence upon particle-particle interactions for weakly inertial particles ($\text{Re} \lesssim 1$) has not been so well studied.

B. Numerical method

Within the IBM method employed, an indicator function

$$\chi = \begin{cases} 1 & \text{if } \mathbf{x} \in \Omega_f \\ 0 & \text{if } \mathbf{x} \notin \Omega_f \end{cases} \quad (5)$$

denotes the locations of fluid and particles phases, with particles contained in volumes denoted by Ω_f . The discretization of the domain results in some grid cells containing both phases which results in the average indicator function for that cell to lie between 0 and 1. The particles were cohesionless, solid, and impermeable spheres with a no-slip velocity boundary condition on their surface. There was no flux of density through the particles, consistent with our conceptual model of Sc representing relative substance, not heat, diffusivity.

The rectangular domain had extent L_x and L_y in the horizontal, and L_z in the vertical. The specific values of these lengths depended upon the number of particles and their geometric configuration. In the horizontal, periodic boundary conditions were used to remove the influence of wall drag. The upper and lower boundary conditions were free-slip for velocity and the values of density at the top and bottom were kept fixed. The domain was discretized into a uniformly spaced grid with equal grid sizes in each dimension: $\Delta x = \Delta y = \Delta z$. As confirmed by tests of settling velocity as it depended on grid resolution (see Appendix A), the particles were sufficiently resolved with at least 16 grid points across the particle diameter.

In most simulations with a horizontal row or planar array of particles, the top of the domain was situated at $z = 10D_p$; in simulations with a three-dimensional array of particles the top of the domain was at $z = 30D_p$. Particles were initialized close to the top of the domain with the lowest particles initially around $z = 0$ where the background density was ρ_0 . The lower boundary was situated sufficiently below the initial position of particles so as to allow the particles to settle and interact before reaching the bottom.

The governing equations were evolved using a three-step Runge-Kutta scheme for convective terms and a second-order Crank-Nicholson scheme for the viscous terms. The particle motions were evolved using the method of Kempe and Fröhlich [40] who made improvements on the algorithm of Uhlmann [38]. Particle-particle interaction forces were composed of a hydrodynamic lubrication force and direct contact forces. Spatial derivatives were performed using second-order finite differences. An in-depth presentation of the numerical model can be found in Biegert *et al.* [35].

C. Single-particle deceleration

Given a sufficiently deep domain with uniform stratification, particles will eventually settle to their equilibrium depth where the surrounding fluid density is equivalent to the particle density. From the definition of the Reynolds and Froude numbers, this distance, z_{eq} , below the reference height at $z = 0$ is

$$z_{\text{eq}}/D_p = 18 \frac{\text{Fr}^2}{\text{Re}}. \quad (6)$$

With $\text{Fr} = 2$ and $\text{Re} = 1/4$, this puts the equilibrium depth at $z_{\text{eq}} = -288D_p$, well below the bottom of the domain in all simulations reported upon here. Although the particles are negatively buoyant through the duration of simulations, the gradual increase in background density nonnegligibly reduces the magnitude of the particles' buoyancy as they settle, contributing to a slowing of their settling speed. This slowing is accounted for in our analysis of the influence of clustering and induced ambient motion upon settling speeds.

Neglecting wake effects, the depth-dependent velocity of a single particle can be estimated assuming an individual particle settles at speed αw_s when the background density is ρ_0 (at $z = 0$). The constant, α , accounts for change from the Stokes settling speed for a weakly inertial particle. In particular, simulations of single-particle settling in uniform density fluid give $\alpha \simeq 0.93$ for $\text{Re} = 1/4$. Neglecting the possible influence of buoyancy associated with fluid carried in a particle's wake, the settling velocity for a particle at depth z is

$$w_{s1}(z) = -\alpha \frac{1}{18} g \frac{\rho_p - \rho(z)}{\rho_0} \frac{D_p^2}{\nu} = -\alpha w_s - z/\tau^*, \quad (7)$$

in which

$$\tau^* = \left[\frac{\alpha}{18} \frac{N^2 D_p^2}{\nu} \right]^{-1} = \frac{18}{\alpha} \frac{\text{Fr}^2}{\text{Re}} \tau. \quad (8)$$

Writing $w_{s1} = dz/dt$ in Eq. (7) and solving the differential equation for particle position, $z(t)$, gives

$$z(t) = -\alpha w_s \tau^* (1 - e^{-t/\tau^*}) + z_0 e^{-t/\tau^*}, \quad (9)$$

in which we have assumed the particle is situated initially at height z_0 . Hence, the speed of the descending particle decreases exponentially in time with e -folding scale τ^* according to

$$w_{s1}(t) = -(\alpha w_s + z_0/\tau^*) e^{-t/\tau^*}. \quad (10)$$

In uniform density fluid, $\tau^* \rightarrow \infty$. As expected, in this limit Eq. (9) reduces to $z(t) = -\alpha w_s t$ and Eq. (10) reduces to $w_{s1}(t) = -\alpha w_s$.

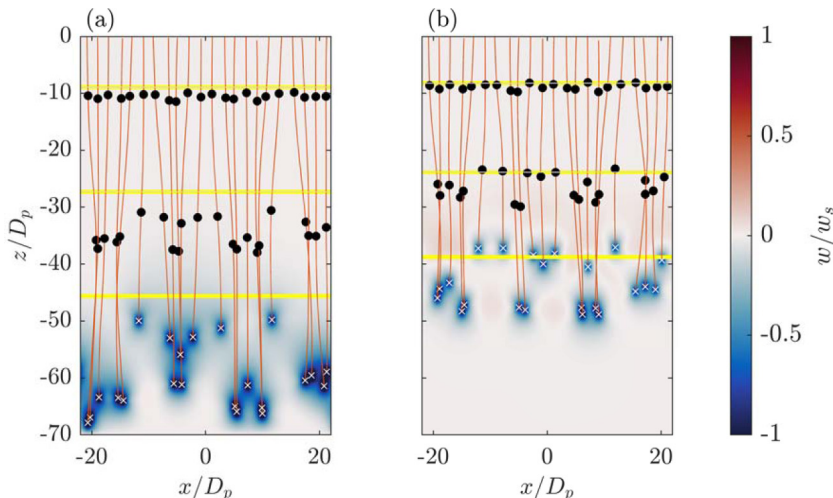


FIG. 1. Tracks of the particle positions in simulations with (a) $Fr = \infty$ and (b) $Fr = 2$. White crosses denote the particle positions at $t/\tau = 50$; black dots denote particle positions at $t/\tau = 10$ and 30 . Horizontal yellow lines indicate the depths of a single particle at times $t/\tau = 10, 30$, and 50 , as determined using Eq. (9). The color field shows the vertical velocity at $y = 0$ and $t/\tau = 50$.

III. HORIZONTAL ROW OF PARTICLES

As the starting point before examining more complex settling configurations, we examine the descent of an initially nearly equally spaced horizontal row of particles aligned along the x axis about $y = z = 0$. The particles spanned the entire horizontal length of the domain, $L_x = sN_p$, where N_p is the number of particles and s is the mean distance between adjacent particles. Using the periodicity of the horizontal boundary, the particles and boundary were positioned so that the unperturbed distance between particles across the periodic boundary was also s . The spanwise length of the domain was $L_y = 20D_p$. Although domains with greater spanwise extent led to increased settling speeds, the dynamics of the settling row remained unchanged. The height of the domain ranged from $z = -70D_p$ to $10D_p$. The particles were randomly perturbed from a regular center-to-center spacing of $2D_p$ both vertically and laterally in the x - z plane with Gaussian noise of amplitude $0.3D_p$. The initial positions of the particles calculated in this way were used in all simulations with different Froude numbers. Here we focus upon the result of simulations with $N_p = 22$ particles settling in unstratified fluid ($Fr = \infty$) and in stratified fluid with $Fr = 2$, as shown in Fig. 1.

In unstratified fluid, the particles segregated as they settled either to form clusters containing three to five particles or to become isolated, consistent with Crowley [32]. Variations in the number of particles in the clusters were due to the relatively sizable initial perturbations of the particles from equally spaced positions. As expected, the vertical velocity of fluid surrounding particle clusters was more negative and the clusters settled faster than the isolated particles. Furthermore, the clusters and isolated particles settled faster than the settling speed of a single particle. For example, all the particles at $t/\tau = 50$ lie below the lowest yellow line in Fig. 1(a), indicating the depth of a single particle at this time. At $t/\tau = 50$ the speed of the leading cluster was 1.8 times the speed of an individual particle.

While similar observations are made for the simulation with stratified fluid [Fig. 1(b)], there are several qualitative differences. Even for a single particle, its settling speed becomes smaller as it descends into more dense ambient fluid. Neglecting wake effects, its predicted speed is given by Eq. (10). Particle clusters were found to descend faster than the speed predicted for a single particle. In particular, in the simulation with $Fr = 2$, the speed of the leading cluster at $t/\tau = 50$ was 1.6 times that of a single particle at this time. Unlike the simulation with unstratified fluid,

trailing particles descended more slowly than the predicted speed of a single particle. The relative reduction in these settling speeds is attributed to the ambient fluid having upward velocity between and in the lee of the particle clusters.

This pair of simulations reveals an important qualitative difference between settling in unstratified and stratified fluid. Whereas in unstratified fluid the ambient response to the settling particles is to rise laterally around flanks of the particles, in stratified fluid the ambient fluid rises in between the descending particle clusters, slowing their advance and separating trailing particles from leading particle clusters.

Both simulations show that clusters of three to five particles form. In a much deeper domain, it seems likely that a secondary aggregation stage could occur whereby neighboring clusters combine due to their mutual interaction, similar to that between individual particles at early times. Because the spacing of these clusters is larger than the initial particle spacing, this would take longer than the initial cluster stage and would require much greater depths to observe. A study of this continuing aggregation lies beyond the scope of the work presented here.

IV. HORIZONTAL AND VERTICAL PLANAR ARRAYS OF PARTICLES

Here we examine the settling of particles situated initially either in a horizontal or vertical planar array. A horizontal array of $N_p = 400$ particles were initially situated about $z = 0$ on a 20 by 20 grid in a domain of size $L_x = 40D_p$ and $L_y = 40D_p$. In the vertical, the domain ranged from $z = -50D_p$ to $z = 10D_p$. The mean particle separation in the x and y directions was $s = 2D_p$. So that the initial condition was truly two-dimensional, the initial positions of the particles were randomly perturbed horizontally but not vertically using a Gaussian random variable with standard deviation $0.3D_p$.

To examine particle clustering, the horizontal cross-section of the domain was discretized into a coarse grid of 20×20 cells and the depth of the lowest particle within each cell in time was recorded. Figure 2 shows snapshots of this map at two times for simulations with unstratified fluid ($Fr = \infty$) and uniformly stratified fluid with $Fr = 2$. In both simulations the particles grouped into clusters interspersed with areas of few or no particles. However, in unstratified fluid the deepest clusters were larger and fewer, each containing more particles than the deepest clusters that formed in the simulation with $Fr = 2$. This is particularly evident in plots showing the vertical velocity in a horizontal cross-section taken $3D_p$ above the lowest particle superimposed with the horizontal positions of particles situated vertically within $3D_p$ of this level [Fig. 2(c) and 2(f)]. As with the case of a row of particles, the ambient stratified fluid responded to the downward motion of the leading clusters by creating broad regions of upward flow between the clusters. In stratified fluid this had the effect of slowing the relative descent of clusters and inhibiting their aggregation to larger size. In both simulations the lowest particles descended much faster than the speed of a single particle at the same depth, as predicted by Eq. (7). At $t/\tau = 24$, the mean speed of the lowest particles in unstratified fluid was 2.4 times that of a single particle, whereas in simulations with $Fr = 2$, the mean speed of the lowest particles was 1.8 times the single-particle speed.

To quantify the growth of clusters in time, we adapted the analysis method of [41], who examined the clustering statistics of a three-dimensional suspension. Here we compute the horizontal radial pair distribution function, defined by

$$G_h(r) = \frac{L_x L_z}{N_p(N_p - 1)} \sum_{m=1}^{N_p} \sum_{n=1, m \neq n}^{N_p} \frac{1}{\Delta A(r)} H\left(\frac{\Delta r}{2} - |r - r_{h,mn}|\right), \quad (11)$$

in which $\Delta A(r) = \pi[(r + \Delta r/2)^2 - (r - \Delta r/2)^2]$ is the area of the circular annulus of radius r , $r_{h,mn} = \sqrt{(x_m - x_n)^2 + (y_m - y_n)^2}$ is the horizontal distance between particle m and n , and H is the Heaviside function. The distance $r_{h,mn}$ includes the contribution of particles across the periodic boundaries through a mirroring of the time-evolving particle positions. An appropriate value of the radial bin size was found to be $\Delta r = D_p/2$ so that the distributions were independent of Δr but were adequately partitioned to observe pairwise structures.

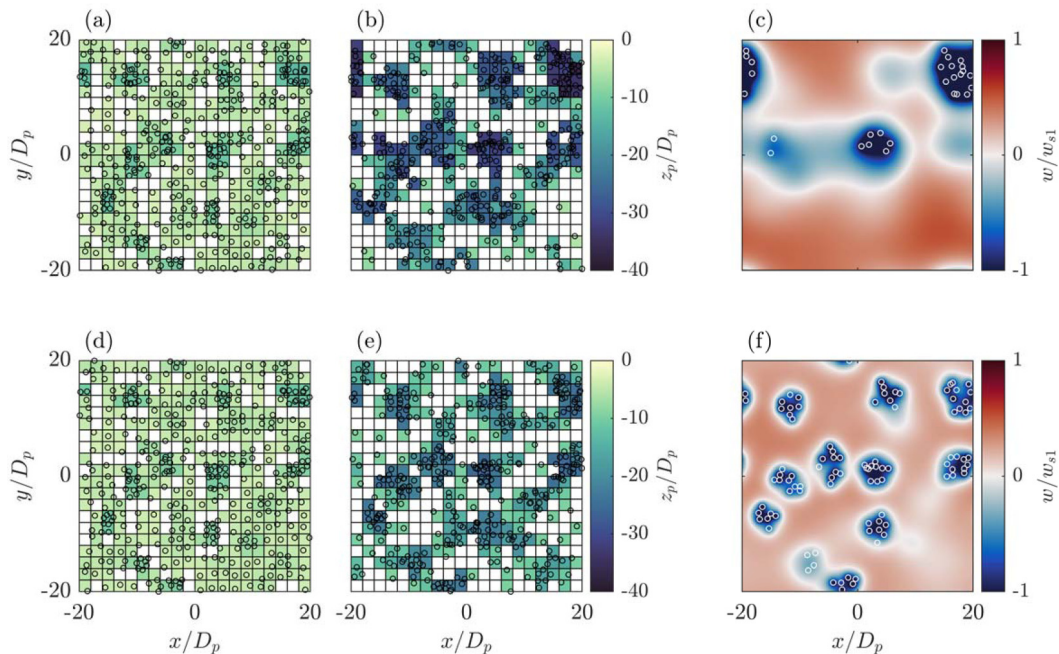


FIG. 2. Location of particles for a horizontal array of 400 particles setting in simulations with $Fr = \infty$ (top row) and $Fr = 2$ (bottom row) shown at times $t/\tau =$ (a, d) 12 and (b, e) 24. Circles indicate the horizontal position of each particle and colors indicate the depth of the lowest particle in each cell. The rightmost plots (c, f) show the normalized vertical velocity at $t/\tau = 24$ with the horizontal cross-section taken $3D_p$ above the lowest of all particles [at $z/D_p = -33.6$ in (c) and at $z/D_p = -23.0$ in (f)]; superimposed white squares show the horizontal position of particles lying vertically within $3D_p$ of the cross-section. The vertical velocity is normalized by the velocity of a single particle according to Eq. (7).

Figures 3(a) and 3(b) show the space-time plots of G_h for the horizontal array of particles shown in Fig. 2, corresponding to $Fr = \infty$ and $Fr = 2$, respectively. At early times the near-uniform initial particle spacing is evident as vertical bands, with each band corresponding to successive nearest-neighbor distances of particles on a square grid. Particle clustering becomes evident after time $t \simeq 8\tau$, when G_h is dominated by a single peak near $r/D_p \approx 1$. Importantly, after $t/\tau \simeq 15$, G_h was statistically stationary and the clusters did not grow in horizontal extent. The average, \bar{G}_h , of G_h from $t = 20\tau$ to 25τ is shown in Fig. 3(c). In the statistically stationary state, the mean extent of the clusters is measured using the first local minimum after the peak of \bar{G}_h . For $Fr = \infty$, this was $\simeq 6.8D_p$, moderately larger than the extent of $5.3D_p$ measured in the simulation with $Fr = 2$.

In separate simulations (not shown), increasing the initial particle separation resulted in the particles behaving more independently, resulting in an increase in the time for cluster formation and a reduction in the settling speed of the lowest particles. Compared to the time of 8τ for clusters to begin to form given an initial particle separation of $s = 2D_p$ (Fig. 3), for $s = 4D_p$, clustering in unstratified fluid did not begin until $t \simeq 40\tau$, a fivefold increase in time.

Whereas upward ambient motion through the particle pack necessarily must occur for a horizontal array, the ambient flow can rise laterally around a vertical array. Furthermore, through the process of drafting, a leading particle can capture a trailing particle in its wake, as has been studied for a particle pair at moderate [$O(10)$] Reynolds number [25,26]. Both processes have the potential to enhance particle cluster settling speeds. The initial array in our study consisted of 4 vertically stacked rows of 11 particles with mean horizontal and vertical spacing of $s = 2D_p$ and lying in

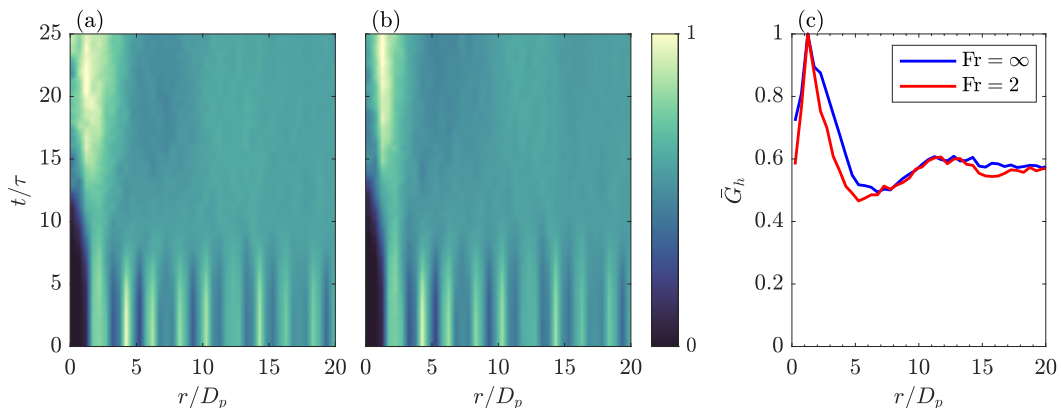


FIG. 3. From simulations shown in Fig. 2, time series of the radial distribution function, G_h , in simulations with (a) $Fr = \infty$ and (b) $Fr = 2$, and (c) the corresponding radial dependence of G_h averaged in time for $20 \leq t/\tau \leq 25$ for $Fr = \infty$ (blue) and $Fr = 2$ (red).

the vertical plane at $y = 0$ between $z = -3D_p$ and $z = 3D_p$. From a regularized grid, each particle was perturbed in the x - z plane by a random number from a Gaussian distribution with standard deviation $0.3D_p$. No perturbations were made in the spanwise direction so that the particles started and remained in the plane $y = 0$ as they settled. The domain size was $L_x = L_y = 22D_p$ in the horizontal and ranged from $z = -70D_p$ to $10D_p$ in the vertical. Although the top row of particles was initially closer to the upper boundary than in the simulations with a single row of particles, the proximity of the upper boundary was found to have little effect on the settling dynamics.

Figure 4 shows a pair of snapshots of particle positions from each of two simulations, one with unstratified fluid and the other with uniform stratification given by $Fr = 2$. The vertical velocity field in the particle plane at both times is also shown. In both simulations, shortly after the particles descended, a particle front was observed to compactify [Figs. 4(a) and 4(c)]. Rapidly the lower particles came into contact and, over time, the front became horizontally nonuniform [Figs. 4(b) and 4(d)] eventually forming clusters. As anticipated, owing to the higher particle concentrations in the lowest clusters, they settled even faster compared with a single particle than in the simulations with a row or horizontal plane of particles. In uniform density fluid the lowest clusters settled $\simeq 2.6$ times faster and in stratified fluid with $Fr = 2$ they settled $\simeq 2.2$ times faster than a single particle at the same depth.

In unstratified fluid, the vertical velocity in the plane of the particles was predominately negative with the ambient flow rising laterally around the clusters (not shown). Consequently, even the trailing particles descended faster than a single particle, as in the case of a settling row of particles. However, in stratified fluid with $Fr = 2$, regions of upward velocity developed between the particle clusters, and the trailing particles moved more slowly than a single particle. This opposing motion restricted the amalgamation of particles into the lowest clusters. Whereas the largest cluster in the case with $Fr = \infty$ had 10 or 11 particles, in the stratified case it was 6–8.

V. THREE-DIMENSIONAL PARTICLE ARRAY

The results of the previous sections have provided an intuition for the settling of particles in a variety of idealized configurations. In particular, we have shown that in stratified fluid upflows develop between particles which restricts the growth of clusters and slows their descent speed relative to what occurs in unstratified fluid. These observations set the stage for the focus of this study, which is the examination of the settling of a randomly dispersed, three-dimensional array

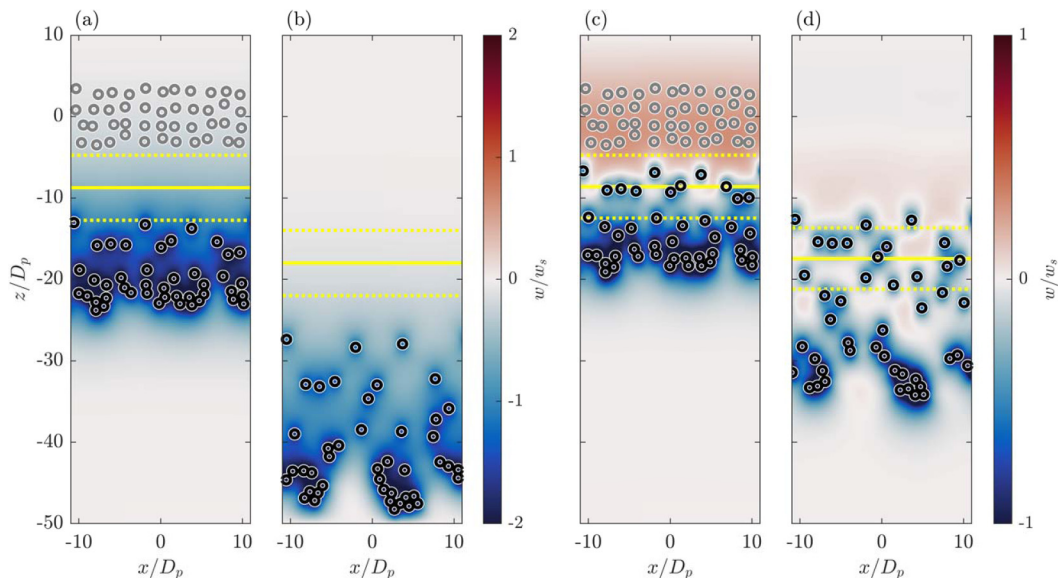


FIG. 4. Snapshots of the settling of a vertical planar array of particles in simulations with $Fr = \infty$ at $t/\tau =$ (a) 10 and (b) 20, and in simulations with $Fr = 2$ at $t/\tau =$ (c) 10 and (d) 20. The initial position of particles is indicated by gray circles in panels (a) and (c). Colors show the vertical velocity of the ambient fluid in the $y = 0$ plane at both times, with values for $Fr = \infty$ indicated to the right of panel (b) and values for $Fr = 2$ indicated to the right of panel (d). Yellow lines indicate the predicted depth at the corresponding times of a single particle settling initially from $z = 0$ (solid) and $z = \pm 4D_p$ (dotted).

of particles, a problem which is relevant to most industrial and environmental problems. Although Doostmohammadi and Ardekani [41] previously studied the settling of a suspension of particles through linearly stratified fluids, their analysis was concerned with particles situated throughout the entire fluid. Here we examine a localized settling particle layer because this better represents the initial process of settling from particle-bearing fluid overlying a more dense particle-free layer.

Two suites of simulations with three-dimensional arrays are presented here, one in which the ambient fluid is uniformly stratified or has uniform density, and the other in which a uniformly stratified layer overlies a uniform density later. The latter study is intended to explore the microscopic dynamics associated with particle-driven convective instability at the base of a stratified layer, as in experiments and simulations of particles passing through a stratified interface overlying uniform density fluid [13–15].

In most simulations the domain had a horizontal extent of $L_x = L_y = 30D_p$ and a vertical extent ranging between $-70D_p$ and $30D_p$. Using a uniform probability distribution, the initial positions of the particles was set by randomly distributing particles between $z = 0$ and $z = H_p \equiv 30D_p$. Overlapping particles was forbidden. Here the number of particles was characterized by a prescribed volume fraction, ϕ , so that the number of particles was $N_p = \lfloor \phi L_x L_y H_p / V_p \rfloor$, in which V_p is the volume of a single particle, and the symbol $\lfloor \cdot \rfloor$ denotes the round-to-the-nearest-integer operator. Explicitly, the number of particles was $N_p = 52$ and 258 for the volume fractions $\phi = 0.001$ and $\phi = 0.005$, respectively. Because of the high computational cost of cases with $\phi = 0.01$, the horizontal extent was $L_x = L_y = 20D_p$, and $N_p = 229$. Although the domain was narrower, the increase in particle density still allowed for sufficient particle interactions to occur. Once a set of initial particle positions was created for a given volume fraction, that set of positions was used for all following simulations with that volume fraction. In most simulations, the relative diffusivity was set by $Sc = 7$. However, some computationally intensive, higher resolution

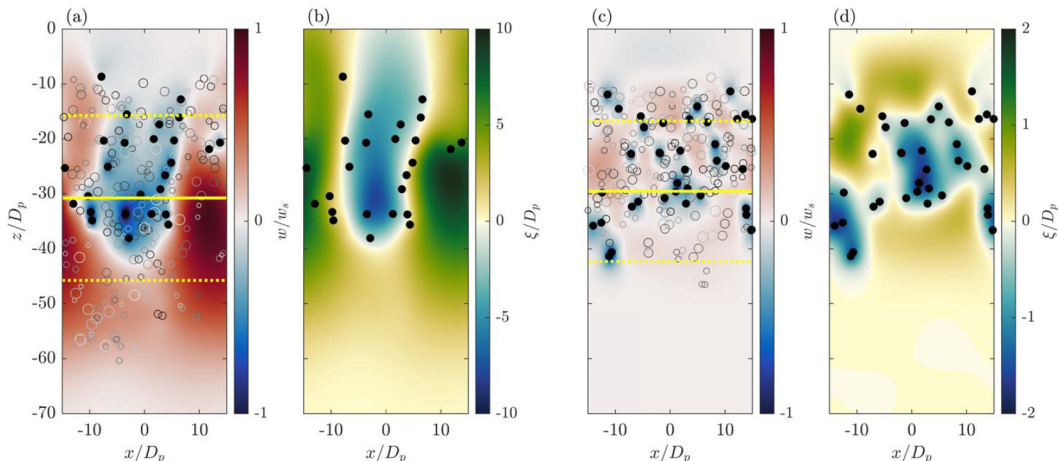


FIG. 5. Snapshots of particle positions at $t/\tau = 50$ in simulations of a settling three-dimensional particle layer with (a, b) $Fr = \infty$ and (c, d) $Fr = 2$. Solid black circles indicate particles lying within $2D_p$ of the midplane at $y = 0$. In (a, c) open circles become lighter gray toward the front and back of the domain in the y direction, with circles being larger toward the front and smaller toward the back. The colored fields show (a, c) the vertical velocity and (b, d) the vertical displacement of fluid in the midplane at $y = 0$. Yellow lines in panels (a) and (c) indicate the predicted depth at the corresponding times of a single particle settling initially from $z = 15$ (solid) and $z = 0$ and $30D_p$ (dotted). In both simulations the initial volume concentration of particles is $\phi = 0.005$.

simulations were performed with $Sc = 70$ to examine the influence of reduced ambient fluid diffusivity.

A. Settling in unstratified and uniformly stratified fluid

As in the previous sections, we begin by comparing results from simulations of particle settling in unstratified fluid and in stratified fluid with $Fr = 2$. Figure 5 shows snapshots from these simulations taken at $t/\tau = 50$. Though all the particle positions are shown in Figs. 5(a) and 5(c), we focus upon the particles lying within $2D_p$ of the $y = 0$ plane (plotted as black circles in all plots). The colored fields show the relative vertical velocity, w/w_s , and relative fluid displacement, ξ/D_p , in the $y = 0$ plane at $t/\tau = 50$. In Fig. 5(b), ξ represents the vertical displacement of fluid from its initial position; in Fig. 5(d), ξ represents the vertical displacement of fluid from its neutral buoyancy level. Particularly striking in the case of uniform density fluid [Figs. 5(a) and 5(b)] is the descent of particles near $y = 0$ mostly in a single plume in the midplane where the vertical velocity and fluid displacement are both downward. On either side of this plume the vertical velocity and fluid displacement is upward. In contrast, there is less coherence in the vertical velocity and displacement fields in the simulation with $Fr = 2$ [Figs. 5(c) and 5(d)]. While most particles near $y = 0$ lay in regions of downward-displaced fluid, the vertical velocity is upward in some of these regions, indicating a rebound in response to the fluid's relative buoyancy. As found in the previous sections, this acts to separate and disperse coherent clusters.

Because the particles are vertically stacked as well as horizontally distributed, one might expect the lowest particles to settle relatively faster than in the case of a horizontal planar array. However, the simulations of a three-dimensional layer show that the mean speed of the lowest particles (laying within $6D_p$ of the particle at greatest depth) is only 1.5 times faster than a single particle in unstratified fluid and 1.1 times faster than a single particle at that depth in stratified fluid. Even in the simulation with unstratified fluid, the uppermost particles descended less quickly than a single particle, as evident from the particles lying above the top dotted yellow line in Fig. 5(a).

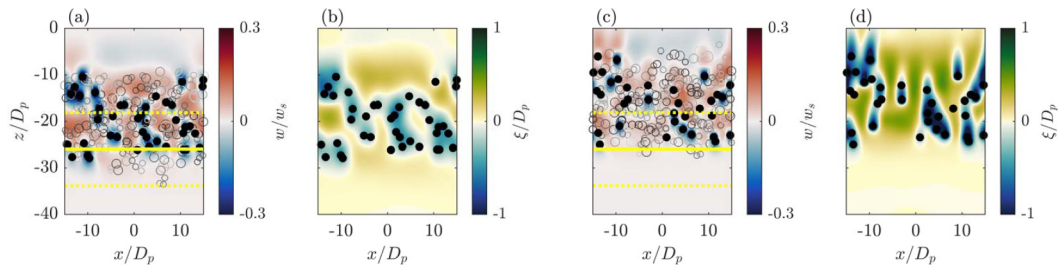


FIG. 6. As in Fig. 5 but for simulation snapshots at $t/\tau = 50$ with $Fr = 1$ and (a, b) $Sc = 7$ and (c, d) $Sc = 70$. In both simulations the initial volume concentration of particles is $\phi = 0.005$.

This demonstrates that the upflows surrounding descending clusters act to disperse the particles vertically and to slow their descent.

In simulations with $Fr = 1$, we further explored the influence of the relative diffusivity of the fluid, as expressed by the Schmidt number. As in Fig. 5, Fig. 6 shows snapshots of the vertical velocity and vertical displacement in the midplane ($y = 0$) as well as the particle positions near the midplane in simulations with the standard setting of $Sc = 7$ [Figs. 6(a) and 6(b)] and with $Sc = 70$ [Figs. 6(c) and 6(d)]. Having a larger Schmidt number means that relatively less dense fluid carried downward in the viscous boundary layer surrounding each particle and in their trailing wake takes longer to diffuse into the surrounding denser ambient fluid. Consequently, the effective density of the particle including this surrounding and trailing fluid is reduced. In comparison with the simulation with $Sc = 7$, the influence of lower diffusivity is evident in the lower vertical velocity magnitudes surrounding the particles [Fig. 6(c)] and the greater vertical displacement of fluid from its neutral buoyancy level [Fig. 6(d)]. These results are consistent with the simulations of Doostmohammadi *et al.* [22] who found that an increase in the Schmidt number led to greater deformation of isopycnals due to reduced diffusion of the deformation. Although Fig. 19 of Ref. [22] demonstrates that the deformation remains within a narrow wake above the settling particle, the presence of many particles passing through the deformed stratification may widen this deformation, so attracting neighboring particles.

We now present diagnostics aimed to quantify the settling and clustering behavior of particles in a range of simulations with varying particle concentration (ϕ), stratification (set by Fr), and relative diffusivity (set by Sc). We first explore the influence upon the relative settling speed of the particles as a whole as well as of the lowest particles, lying with $6D_p$ of the bottom-most particle at each time. These analyses are shown in Fig. 7. The descent of the particles as a whole is determined by the speed of the center of mass of all the particles. This is plotted relative to the predicted (time-dependent) speed of a single particle, given by Eq. (10). In simulations with strong stratification, the center-of-mass speed rapidly became 20% smaller than the speed of a single particle, though it gradually increased in time. The volume concentration, ϕ , had little influence upon the center of mass speed, at least for concentrations below 0.01 [Fig. 7(a)]. However, the clusters at the bottom descended faster if ϕ was larger, owing to stronger particle-particle interactions occurring when the particles initially were in closer proximity [Fig. 7(c)].

Stratification had the strongest influence upon the settling speed of both the center of mass and the lowest particles, as shown in Figs. 7(b) and 7(d). In a uniform density fluid ($Fr = \infty$), the center of mass gradually accelerated over time, whereas its speed remained close to that of a single particle in simulations with $Fr = 4$ and $Fr = 2$. In the case with strong stratification ($Fr = 1$), the particles first collectively slowed down relative to a single particle before gradually increasing in speed. A stronger wake effect in fluid with lower diffusivity ($Sc = 70$) is evident from the relatively slower speed. At $t/\tau = 5$, the relative center of mass speed is 0.73 compared to the simulation with $Sc = 7$ for which the relative speed is 0.83. Acceleration of the lowest particles was evident in all simulations with $Sc = 7$. However, in the simulation with the strongest stratification ($Fr = 1$) and

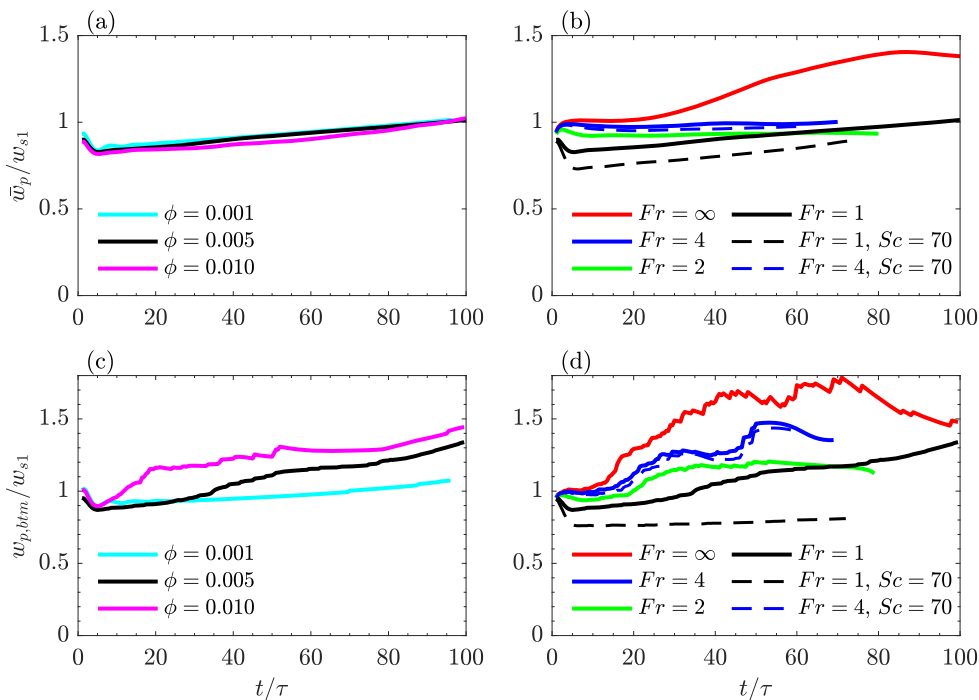


FIG. 7. Particle center-of-mass relative settling speed over time for (a) different volume fractions with $Fr = 1$ and (b) different Froude numbers with $\phi = 0.005$, and the relative mean settling speed of the particles within $6D_p$ of the lowest particle for (c) different volume fractions with $Fr = 1$ and (d) different Froude numbers with $\phi = 0.005$. Speeds are normalized by the time-dependent speed, w_{s1} , predicted for a single particle by Eq. (10).

with $Sc = 70$, the lowest particles settled at near-constant speed, approximately 0.8 of the speed of a single particle. This is a result of these particles carrying buoyant fluid down with them in their wake and, because the diffusivity was lower, this provided a significant retarding force on the particle clusters.

The settling speed of particle clusters was also examined by Doostmohammadi and Ardekani [41], who likewise noted a decrease in the mean settling speed with increasing Froude number, although their study involved larger Froude numbers ($Fr \geq 12$) and generally a smaller number of particles ($N_p = 8$ to 64) distributed throughout a triply periodic domain. Notably, they found that the mean settling speed became near-constant after a transient startup time, as opposed to our study that shows a gradual increase in the descent speed over time in all cases with $Sc = 7$. We attribute this to the presence of a settling front in our simulations whereby the lowest particles descend without the influence of wake-effects induced by underlying particles. This is why the mean descent speed of the leading particles [Fig. 7(d)] is faster than the mean speed of all the particles [Fig. 7(b)].

One measure of the formation of clusters is through computing their horizontal displacement from their initial positions while settling. Specifically, at each time we compute the root-mean-square horizontal displacement of all the particles:

$$\langle d_p \rangle = \sqrt{\sum_{N_p} \{ [x_n - x_n(t=0)]^2 + [y_n - y_n(t=0)]^2 \}}. \quad (12)$$

This is plotted in Fig. 8 as it depends upon the change in depth, $\bar{z} - z_0$, of the center of mass of the particles from the initial position of the center of mass, at z_0 . In all cases the rate of

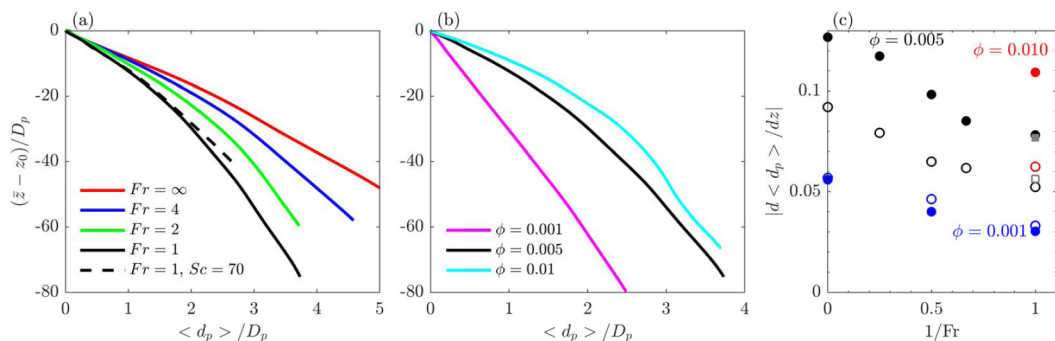


FIG. 8. Root-mean-square horizontal displacement of particles as it depends upon the depth below the initial location, $\bar{z} - z_0$, of the particles' center of mass in simulations with (a) $\phi = 0.005$ and different Fr, as indicated, and (b) Fr = 1 and different ϕ , as indicated. (c) The magnitude of the rate of change of $\langle d_p \rangle$ with depth measured between $\bar{z} - z_0 = -4$ and -6 (solid symbols) and between -24 and -26 (open symbols) as it depends upon the inverse Froude number and initial concentration with $\phi = 0.01$ (red circles), $\phi = 0.005$ (black circles), and $\phi = 0.001$ (blue circles). The gray symbols correspond to Fr = 1, $\phi = 0.005$, and Sc = 70.

change of $\langle d_p \rangle$ with depth was largest in unstratified fluid, being smaller in simulations with larger stratification or smaller particle concentration, and as the particles descended to greater depth. In particular, in simulations with Fr = 1, the mean displacement was approximately half that of particle in unstratified fluid by the time the particles descended by $50D_p$. The mean displacement was relatively larger if the volume concentration was larger, owing to stronger particle-particle interactions [Fig. 8(b)].

Except in some simulations with $\phi = 0.001$, the rate of change of $\langle d_p \rangle$ with depth became smaller as the particles descended. The early-time influence of stratification upon $\langle d_p \rangle$ is measured by computing the rate-of-change of $\langle d_p \rangle$ with \bar{z} when the particles' center of mass was situated $5D_p$ below its initial location. This is plotted as solid symbols for a range of simulations in Fig. 8(c). The rate of change was also computed when the particles' center of mass was situated $25D_p$ below its initial location, with these values being plotted as open symbols in Fig. 8(c). As anticipated, the displacement increased more with depth if the particle concentration was larger, allowing for stronger particle-particle interactions. At fixed concentration, the increase was 50% larger in

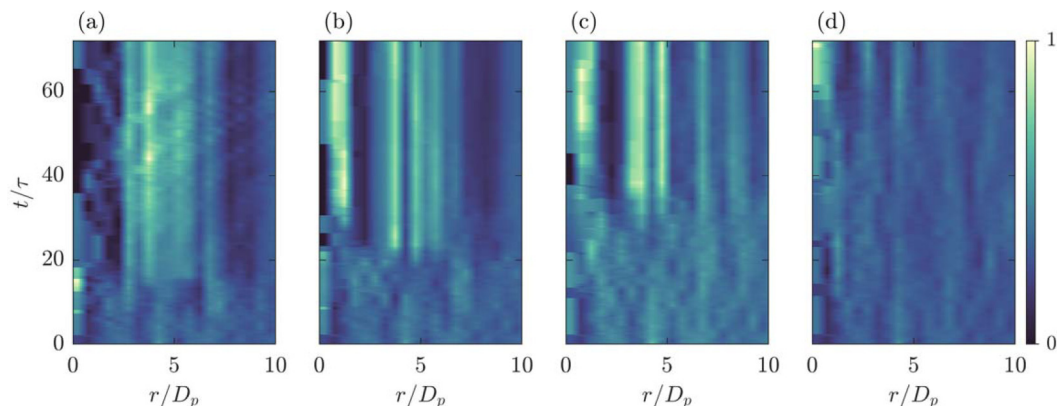


FIG. 9. Particle horizontal radial distribution function for particles within $6D_p$ of the lowest particle, computed from simulations with $\phi = 0.005$, Sc = 7 and (a) Fr = ∞ , (b) Fr = 2, (c) Fr = 1, and with (d) $\phi = 0.005$, Fr = 1 and Sc = 70. The color scale is arbitrary.

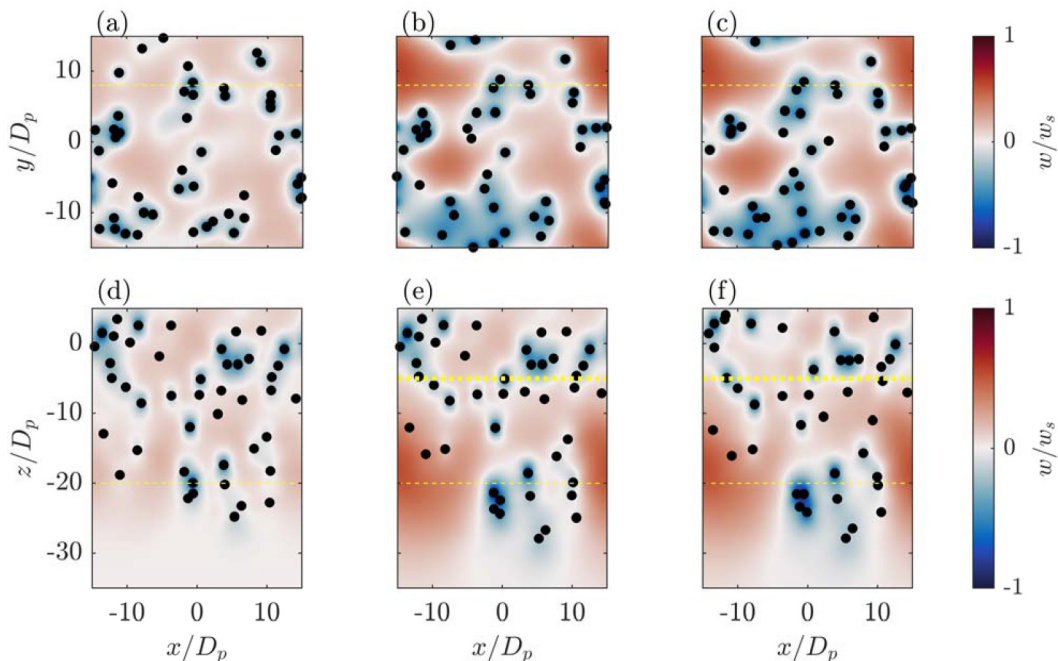


FIG. 10. Cross-sections of vertical velocity at $t/\tau = 30$ from simulations with (a, d) uniform stratification with $Sc = 7$ and $Fr = 2$, (b, e) nonuniform stratification with $Sc = 7$ and $Fr = 2$ above $z/D_p = -5$ with uniform density below, and (c, f) as in panels (b, e) but with $Sc = 70$. The top row of plots shows horizontal cross-sections at $z/D_p = -20$ with circles denoting the horizontal position of particles lying vertically within $2D_p$ of the cross-section; the dashed lines indicating the location of the vertical cross-section in panels (d–f). The bottom row of plots shows vertical cross-sections at $y = 8D_p$ with circles denoting the positions of particles lying within $2D_p$ of the cross-section; the dotted lines in panels (e, f) indicate the location of the base of the stratified layer and the dashed lines indicate the location of the horizontal cross-section in panels (a–c). The color scale for all plots is shown to the right. In all simulations $\phi = 0.005$.

simulations with unstratified fluid compared with simulations having $Fr = 1$. Increasing Sc from 7 to 70 had little effect upon the initial rate of horizontal displacement although it resulted in relatively smaller displacements at shallower depths and larger displacements at greater depths.

As another measure of the formation of clusters over time, we computed the horizontal radial distribution, G_h . Unlike this analysis applied to a horizontal array of particles (Fig. 3), here it was applied only to particles lying within $6D_p$ of the lowest particle. This allowed us to focus on the clustering of the lowest descending particles. A separate analysis of the three-dimensional radial distribution, as performed by Doostmohammadi and Ardekani [41], was found to be less effective at characterizing clustering. This is because the vertical extent of the particle layer decreases in strongly stratified fluid largely as a consequence of the negative buoyancy of particles becoming smaller with depth, as in Eq. (7). Consequently, the three-dimensional radial distribution is dominated by the vertical, rather than horizontal, consolidation of particles.

The horizontal radial distributions computed for four simulations is shown in Fig. 9. In unstratified fluid after $t/\tau \simeq 15$, the distribution peaks for radial separations between $3D_p$ and $6D_p$ [Fig. 9(a)]. In contrast, the simulations of settling in stratified fluid gives narrower peaks at smaller radial separations. In simulations with $Sc = 7$ and $Fr = 2$ and 1, the distributions peak between $D_p/2$ and $2D_p$ these peaks becoming pronounced after $t/\tau \sim 30$ [Figs. 9(b) and 9(c)]. The main peaks at low radial separation are associated with particles in a single cluster. Additional peaks at larger radial separations corresponding to particle separations between neighboring clusters. In

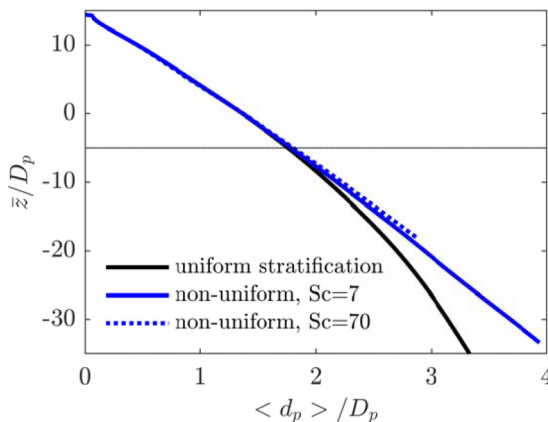


FIG. 11. For the simulations shown in Fig. 10, the root-mean-square of the horizontal particle displacement plotted against the depth of the center of mass of the particles. The horizontal dotted line indicates the depth of the transition from stratified to unstratified fluid at $z/D_p = -5$.

the simulation with $Sc = 70$ and $Fr = 1$ the peak takes longer to develop and is significant for smaller separation distances between 0 and D_p . This is consistent with observations of the particles becoming more vertically aligned if the background diffusion is small.

The comparison between these simulations demonstrates that stratification delays the formation of particle clusters, consistent with the delayed horizontal displacement shown in Fig. 8. Rather than enhancing cluster formation, stratification reduces particle descent speeds and retards long-range particle-particle interactions.

B. Linear-homogeneous background stratification

Here we put our work in context of previous simulations and experiments examining the settling from an upper particle-bearing surface layer into an underlying fluid of uniform density [13–16,42]. Although in those studies the interstitial fluid in the upper layer had uniform density, the interface between the two layers was not infinitesimally thin. Hence, our focus is upon settling through the stratified interface into the underlying uniform density fluid. This was modeled with the background density profile

$$\bar{\rho} = \rho_0 - \gamma \begin{cases} z & z \geq -5D_p, \\ -5D_p & z < -5D_p. \end{cases} \quad (13)$$

The transition between uniform stratification and uniform density fluid was placed $5D_p$ below the lowest particles, situated at $z = 0$, to allow the particles time to accelerate from rest to quasi-steady state within the stratified layer before reaching the uniform density layer. In the studies reported upon here, the volume concentration was taken to be $\phi = 0.005$. For comparison to results in Sec. V A, the domain size and initial particle positions were initially the same as in those simulations with unstratified and uniformly stratified fluid.

For three simulations at $t/\tau = 30$, Fig. 10 shows horizontal cross-sections of the vertical velocity at $z = -20D_p$ ($15D_p$ below the bottom of the interface) and vertical cross-sections of the vertical velocity at $y = 8D_p$. Particles lying within $2D_p$ of these cross-sections are also plotted. In comparison with the uniformly stratified simulation, the cross-sections show there are larger connected regions of downward velocity correlated with the particles near $z = -20D_p$, and the upward velocity between the particle clusters is larger.

The differences between the nonuniformly stratified simulations with $Sc = 7$ and $Sc = 70$ are more subtle. While particles in the lowest clusters are situated in similar locations, the particles

still in the upper stratified fluid are more vertically aligned in fluid with smaller diffusivity, as is particularly apparent in the vertical cross-sections near $(x, z) = (-12D_p, 2D_p)$.

As in Fig. 8, the root-mean-square of horizontal displacement of particles as their center of mass descends in depth was computed in these simulations, and are plotted in Fig. 11. As before, in uniform stratification the rate of horizontal displacement decreases significantly with depth. However, in nonuniform stratification the rate changes little after the particles pass into uniform density fluid. In the simulation with $Sc = 70$ the rate changes even less than in the case with $Sc = 7$ which can be attributed to the interface between stratified and uniform-density fluid diffusing vertically at a slower rate.

VI. DISCUSSION AND CONCLUSIONS

This study was originally motivated by observations of laboratory experiments in which micron-sized particles in a fresh water layer overlying salt water were observed to descend into the saline ambient fluid not as a cloud, but in discrete particle plumes [11–14]. It was hypothesized that particles passing through the continuously stratified interface between the fresh water and saline layers interacted so as to form clusters that then settled collectively into the underlying ambient fluid. Running realistic particle-resolving simulations of these dynamics is presently infeasible due to the large domain size and fine resolution required to capture the motion of thousands of particles at low Reynolds numbers and large Schmidt numbers. For example, modeling 10-micron-diameter glass microspheres settling in salt water would require $Re \simeq 0.01$ and $Sc \simeq 700$.

Our approach has been to gain insight into possible collective settling processes by focusing upon the influence of stratification. The Reynolds number was fixed at $Re = 1/4$, which is representative of the weakly inertial settling of fine sand in water. In test simulations with larger Reynolds numbers (and corresponding larger Froude numbers), there was insignificant difference in settling and displacement rates if $Re = 1$, though initial displacements grew substantially more quickly initially if $Re = 4$ (see Appendix B). This suggests that the choice of $Re = 1/4$ is sufficient to capture the essential dynamics of noninertial settling. In most of our simulations, the Schmidt number was fixed at $Sc = 7$, with corresponding Péclet number of $Pe = 1.75$. In these simulations, any fluid carried to depth in the wake of the descending particle would rapidly diffuse into the surrounding ambient fluid. These neglect the potentially important dynamics of particles being slowed by the buoyant fluid in its wake [39] as well as enhanced particle interactions whereby a trailing particle can be drafted into the wake of a leading particle [25,26]. Consequently, we also performed a small number of computationally intensive simulations having $Sc = 70$.

To gain insight into the influence of stratification upon the interactions of settling particles, we examined the evolution of an initially horizontal row of particles and a horizontal and vertical planar array of particles. In all cases the particles eventually gathered into clusters with isolated particles trailing behind. The main influence of stratification was to create upflows between the clusters which reduced the size of clusters and retarded the advance of both the lowest clusters and trailing particles relative to the descent of a single particle. Similar dynamics were observed in simulations of a three-dimensional layer of particles. For these, clustering was quantified through the consideration of the root-mean-square horizontal displacement of particles as a function of their mean depth as well as the horizontal radial distribution of the particles in the lowest clusters as a function of time. These showed that particles in strong stratification, with $Fr = 1$, deviated horizontally at approximately half the rate of particles in unstratified fluid and that this rate became smaller as the particles descended. While the horizontal radial distribution of the lowest particles in unstratified fluid peaked around 4 particle diameters, the particles were more closely clustered in strong stratification, peaking around 1 particle diameter in simulations with $Sc = 7$. Lower diffusivity resulted in particles being more vertically aligned, reminiscent of the drafting phenomena that has been observed for particle pairs in stratified fluid at moderate Reynolds numbers [25,26]. The clustering of particles into near-vertical alignment in fluid with $Sc = 70$ took longer ($t \gtrsim 60\tau$) than clustering in more diffusive fluid. For this reason, there was little difference in the settling

of particles from a stratified layer into an underlying uniform density fluid because, in these simulations, most of the particles had rained out of the stratified layer by $t/\tau = 20$.

The results presented here suggest that stratification alone is insufficient to explain the observed collective settling behavior in laboratory experiments. Several additional factors should be considered: the low diffusivity of salt water must be better represented with larger Schmidt numbers; the vertical domain size must be sufficiently large to allow for particles to interact within a deep enough stratified layer potentially leading to their columnarization; the horizontal domain size must be larger, and the number of particles correspondingly greater, to capture the horizontal scale of fingers and “leaky ducts” observed in laboratory experiments [11–14]. Based on these experiments, we estimate the minimum vertical and horizontal scales to capture the formation of a leaky duct should be on the order of 1 cm. And so a simulation of particles with diameter $D_p = 10 \mu\text{m}$, would require a $1000D_p \times 1000D_p \times 1000D_p$ domain containing on the order of 10^6 particles at concentrations as low as $\phi = 0.001$. As prohibitive as such simulations would be, particularly with $Sc = 700$, it is hoped that insights into the microscopic dynamics associated with the development of collective particle settling behavior can be gained first by increasing the Schmidt number in smaller domains and then increasing the domain scale.

ACKNOWLEDGMENTS

This research was supported by funding provided by the Natural Sciences and Engineering Research Council of Canada (NSERC) through their Discovery grant program. Simulations were completed on Compute Canada’s high-performance computing clusters Cedar and Graham.

APPENDIX A: RESOLUTION TESTS

To determine the necessary grid resolution for accurate numerical simulations, two sets of simulations with various resolutions were compared: the first corresponds to the settling of a row of particles; the second corresponds to a random, three-dimensional array of particles. Simulations with background stratification were completed to account for the associated effects, such as drag.

In the the first study, an initially horizontal row of particles at $z = 0$ were all equally spaced except for the center particle that was displaced downward. Figure 12(a) shows the settling velocity of this center particle, which exhibited the fastest descent and was the most likely to be influenced by the grid resolution. The settling speed was very similar between the two resolutions with a maximum

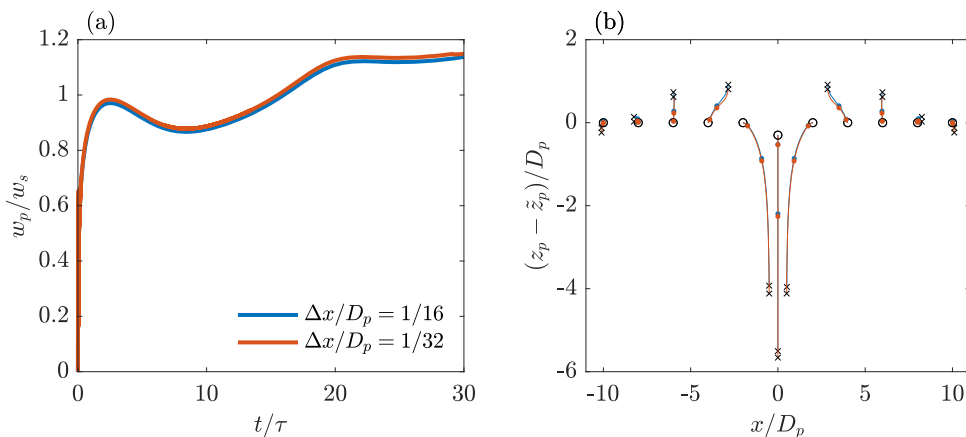


FIG. 12. (a) Settling speed of the center, downwardly perturbed particle and (b) the relative particle positions for a horizontal row of 11 particles with $Fr = 2$.

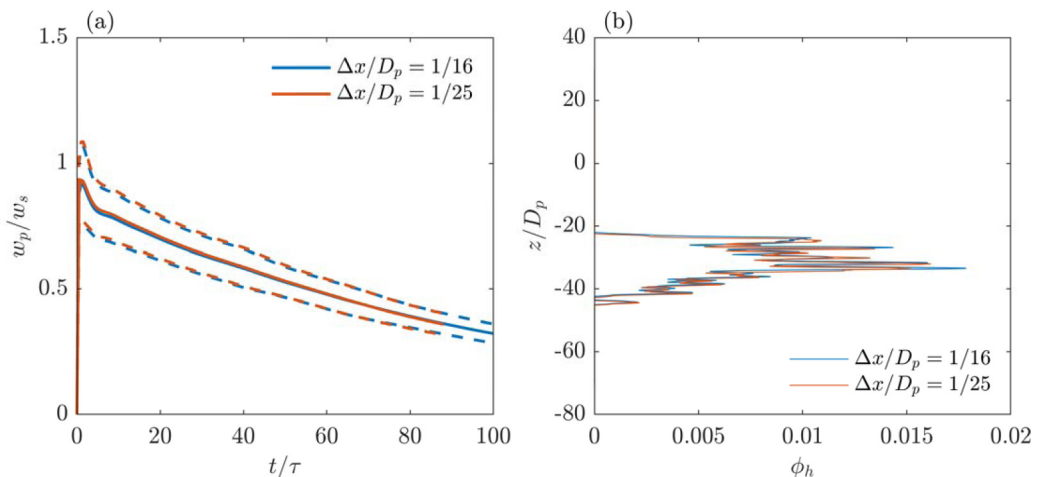


FIG. 13. (a) Mean particle settling speed (the dashed lines are one standard deviation away from the mean). (b) particle volume fraction at $t/\tau = 75$.

difference of 1.5%. The particle positions relative to an unperturbed row are also similar between the two resolution cases [Fig. 12(b)]. Because the difference between the two resolutions was small, the smaller resolution of $\Delta x/D_p = 1/16$ was deemed suitable.

Because the majority of our simulations were completed with a random, three-dimensional array of particles for which the settling dynamics were more complex than that of the horizontal row, we present a resolution test for this configuration as well. The evolution of the mean particle settling velocity and the horizontally averaged particle volume fraction at $t/\tau = 75$ are shown for the case with $Fr = 1$, $\phi = 0.005$, and $Re = 1/4$ (Fig. 13). The maximum difference in the mean settling speed was 1% between the low resolution and high resolution simulations, indicating that at grid size of $\Delta x/D_p = 1/16$ is suitable. Further justification for this resolution is found in Vowinkel *et al.* [36], who used a resolution of $\Delta x/D_{50} = 1/18.25$ in their study on the sedimentation of polydisperse, cohesive sediments.

APPENDIX B: REYNOLDS NUMBER EFFECT

Thus far, a Reynolds number of $1/4$ has been used to model weakly inertial sedimentation. However, particles settling in environmental and industrial flows can have wide-ranging Reynolds numbers. Consequently, an investigation on the effect of Reynolds number is needed.

For fixed particle size, the Reynolds number is changed by varying the density ratio ρ_p/ρ_0 and, hence, the settling velocity. Changing the Reynolds number results in a change in the particle equilibrium depth [as given by Eq. (6)]. To ensure that the changes are a result of inertia and not the variation in settling distance, we fix the settling distance by simultaneously adjusting the Froude number. We set the equilibrium depth to $z_{eq}/D_p = 72$ and varied the Reynolds number between $1/4$ and 4.

Although the range of Reynolds number varied from near the Stokes regime (at low Re) to inertial settling, this range had little effect on the characteristics of the sedimentation (Fig. 14). Even with slight variations in the mean settling speed and mean horizontal displacement, the settling at $Re = 1/4$ was representative of a wider range of Reynolds numbers.

The similarity in these plots may be understood from the relative strengths of stratification to viscosity, as expressed by the ratio Fr^2/Re . Although the viscous component weakened with increasing Re , so did the role of stratification at an equal rate. Although the ratio $Fr^2/Re = 4$ was greater than one, Fig. 14(a) shows that stratification still dominated due to the exponential decay

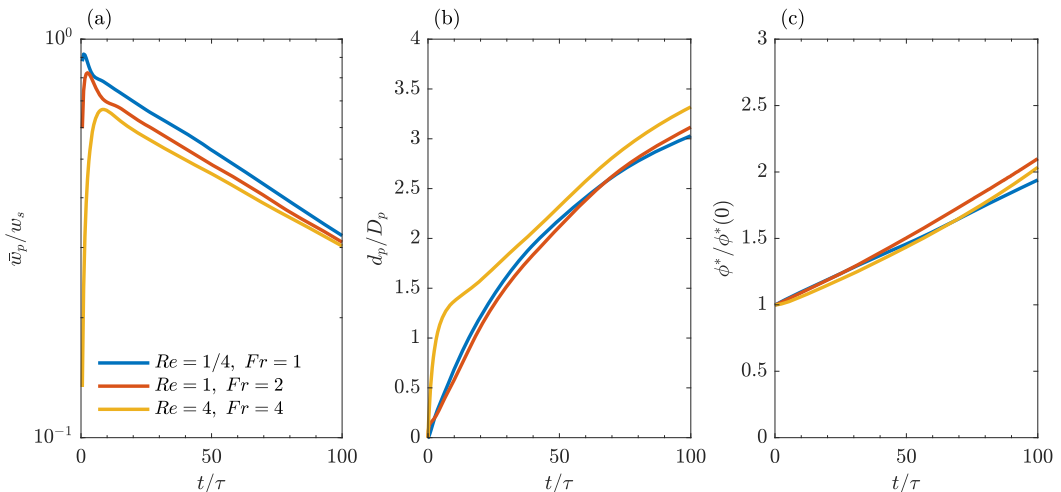


FIG. 14. Reynolds number dependence on (a) mean particle settling speed, (b) RMS particle horizontal displacement, and (c) particle layer volume fraction.

in settling velocity. For $Re = 1/4$ the transition from stratification-dominated to inertial-dominated motion occurred in the range of $Fr = 2 - 3$ corresponding to $Fr^2/Re = 16-36$.

APPENDIX C: BOUSSINESQ APPROXIMATION

The strong stratification case of $Fr = 1$ used in Sec. V resulted in a fluid density difference of $\Delta\rho/\rho_0 \approx 1$ which is outside the Boussinesq limit. However, Doostmohammadi *et al.* [22] had investigated the settling of an individual particle through a linear background density profile and found that there was less than 0.5% deviations between simulations with and without the Boussinesq approximation for stratifications down to $Fr = 0.829$. Although the numerical method of their model was different from the immersed boundary method used here, comparison of the settling velocity of an individual particle at $Fr = 0.829$ was comparable, being 13% different at maximum velocity. Furthermore, although this comparison was made for an individual particle, the addition of multiple particles will not change the applicability of the Boussinesq approximation.

-
- [1] H. Gao and M. K. Stenstrom, Development and applications in computational fluid dynamics modeling for secondary settling tanks over the last three decades: A review, *Water Env. Res.* **92**, 796 (2020).
 - [2] R. Sparks, S. Carey, J. Gilbert, L. Glaze, H. Sigurdsson, and A. Woods, *Volcanic Plumes* (John Wiley, Chichester, UK, 1997).
 - [3] C. Bonadonna and J. C. Phillips, Sedimentation from strong volcanic plumes, *J. Geophys. Res.* **108**, 2340 (2003).
 - [4] T. Kjørboe, J. L. S. Hansen, A. L. Alldredge, G. A. Jackson, U. Passow, H. G. Dam, D. T. Drapeau, A. Waite, and C. M. Garcia, Sedimentation of phytoplankton during a diatom bloom: Rates and mechanisms, *J. Mar. Res.* **54**, 1123 (1996).
 - [5] A. R. Horner-Devine, R. D. Hetland, and D. G. MacDonald, Mixing and transport in coastal river plumes, *Annu. Rev. Fluid Mech.* **47**, 569 (2015).
 - [6] S. MacIntyre, A. L. Alldredge, and C. C. Gotschalk, Accumulation of marines now at density discontinuities in the water column, *Limnol. Oceanogr.* **40**, 449 (1995).

- [7] M. A. McManus, A. L. Alldredge, A. H. Barnard, E. Boss, J. F. Case, T. J. Cowles, P. L. Donaghay, L. B. Eisner, D. J. Gifford, C. F. Greenlaw, C. M. Herren, D. V. Holliday, D. Johnson, S. MacIntyre, D. M. McGehee, T. R. Osborn, M. J. Perry, R. E. Pieper, J. E. B. Rines, D. C. Smith *et al.*, Characteristics, distribution, and persistence of thin layers over a 48 hour period, *Mar. Ecol. Prog. Ser.* **261**, 1 (2003).
- [8] A. B. Burd and G. A. Jackson, Particle aggregation, *Annu. Rev. Marine Sci.* **1**, 65 (2009).
- [9] D. J. Nowacki, A. R. Horner-Devine, J. D. Nash, and D. A. Jay, Rapid sediment removal from the Columbia river plume near field, *Cont. Shelf Res.* **35**, 16 (2012).
- [10] K. R. Scheu, D. A. Fong, S. G. Monismith, and O. B. Fringer, Sediment transport dynamics near a river inflow in a large alpine lake, *Limnol. Oceanogr.* **60**, 1195 (2015).
- [11] J. D. Parsons, J. W. M. Bush, and J. P. M. Syvitski, Hyperpycnal plume formation from riverine outflows with small sediment concentrations, *Sedimentology* **48**, 465 (2001).
- [12] D. Hoyal, M. Bursik, and J. Atkinson, The influence of diffusive convection on sedimentation from buoyant plumes, *Mar. Geol.* **159**, 205 (1999).
- [13] S. D. Jazi and M. G. Wells, Enhanced sedimentation beneath particle-laden flows in lakes and the ocean due to double-diffusive convection, *Geophys. Res. Lett.* **43**, 10,883 (2016).
- [14] B. R. Sutherland, B. Mueller, B. Sjerne, and D. Deepwell, Particle settling from constant-flux surface gravity currents and a near-stationary particle-bearing layer, *Phys. Rev. Fluids* **6**, 063802 (2021).
- [15] P. Burns and E. Meiburg, Sediment-laden fresh water above salt water: Linear stability analysis, *J. Fluid Mech.* **691**, 279 (2012).
- [16] Y.-C. Shao, C.-Y. Hung, and Y.-J. Chou, Numerical study of convective sedimentation through a sharp density interface, *J. Fluid Mech.* **824**, 513 (2017).
- [17] A. N. Srdić-Mitrović, N. A. Mohamed, and H. J. S. Fernando, Gravitational settling of particles through density interfaces, *J. Fluid Mech.* **381**, 175 (1999).
- [18] R. Camassa, C. Falcon, J. Lin, R. M. McLaughlan, and N. Mykins, A first-principle predictive theory for a sphere falling through sharply stratified fluid at low Reynolds number, *J. Fluid Mech.* **664**, 436 (2010).
- [19] N. Abaid, D. Adalsteinsson, A. Agyapong, and R. M. McLaughlin, An internal splash: Levitation of falling spheres in stratified fluids, *Phys. Fluids* **16**, 1567 (2004).
- [20] J. Magnaudet and M. J. Mercier, Particles, drops, and bubbles moving across sharp interfaces and stratified layers, *Annu. Rev. Fluid Mech.* **52**, 61 (2020).
- [21] L. Verso, M. van Reeuwijk, and A. Liberzon, Transient stratification force on particles crossing a density interface, *Int. J. Multiphase Flow* **121**, 103109 (2019).
- [22] A. Doostmohammadi, S. Dabiri, and A. M. Ardekani, A numerical study of the dynamics of a particle settling at moderate Reynolds numbers in a linearly stratified fluid, *J. Fluid Mech.* **750**, 5 (2014).
- [23] B. G. Inman, C. J. Davies, C. R. Torres, and P. J. S. Franks, Deformation of ambient chemical gradients by sinking spheres, *J. Fluid Mech.* **892**, A33 (2020).
- [24] G. Kynch, The slow motion of two or more spheres through a viscous fluid, *J. Fluid Mech.* **5**, 193 (1959).
- [25] L. Wang, Z. L. Guo, and J. D. Mi, Drafting, kissing, and tumbling process of two particles with different size, *Comp. Fluids* **96**, 20 (2014).
- [26] S. Ghosh and M. Kumar, Study of drafting, kissing, and tumbling process of two particles with different sizes and densities using immersed boundary method in a confined medium, *Appl. Math. Comp.* **386**, 125411 (2020).
- [27] D. Deepwell, R. Ouillon, E. Meiburg, and B. R. Sutherland, Settling of a particle pair through a sharp, miscible density interface, *Phys. Rev. Fluids* **6**, 044304 (2021).
- [28] A. Doostmohammadi and A. M. Ardekani, Interaction between a pair of particles settling in a stratified fluid, *Phys. Rev. E* **88**, 023029 (2013).
- [29] K. O. L. F. Jayaweera, B. J. Mason, and G. W. Slack, The behaviour of clusters of spheres falling in a viscous fluid. Part 1. Experiment, *J. Fluid Mech.* **20**, 121 (1964).
- [30] L. M. Hocking, The behaviour of clusters of spheres falling in a viscous fluid. Part 2. Slow motion theory, *J. Fluid Mech.* **20**, 129 (1964).
- [31] P. Ganatos, R. Pfeffer, and S. Weinbaum, A numerical-solution technique for three-dimensional Stokes flows, with application to the motion of strongly interacting spheres in a plane, *J. Fluid Mech.* **84**, 79 (1978).

- [32] J. M. Crowley, Viscosity-induced instability of a one-dimensional lattice of falling spheres, *J. Fluid Mech.* **45**, 151 (1971).
- [33] J. M. Crowley, Clumping instability of a falling horizontal lattice, *Phys. Fluids* **19**, 1296 (1976).
- [34] J. M. Crowley, Clumping instability which is not predicted by the nearest-neighbor approximation, *Phys. Fluids* **20**, 339 (1977).
- [35] E. Biegert, B. Vowinckel, and E. Meiburg, A collision model for grain-resolving simulations of flows over dense, mobile, polydisperse granular sediment, *J. Comput. Phys.* **340**, 105 (2017).
- [36] B. Vowinckel, J. Withers, P. Luzzatto-Fegiz, and E. Meiburg, Settling of cohesive sediment: Particle-resolved simulations, *J. Fluid Mech.* **858**, 5 (2019).
- [37] R. Ouillon, I. A. Houghton, J. O. Dabiri, and E. Meiburg, Active swimmers interacting with stratified fluids during collective vertical migration, *J. Fluid Mech.* **902**, A23 (2020).
- [38] M. Uhlmann, An immersed boundary method with direct forcing for the simulation of particulate flows, *J. Comput. Phys.* **209**, 448 (2005).
- [39] J. Zhang, M. J. Mercier, and J. Magnaudet, Core mechanisms of drag enhancement on bodies settling in stratified fluid, *J. Fluid Mech.* **875**, 622 (2019).
- [40] T. Kempe and J. Fröhlich, An improved immersed boundary method with direct forcing for the simulation of particle laden flows, *J. Comput. Phys.* **231**, 3663 (2012).
- [41] A. Doostmohammadi and A. M. Ardekani, Suspension of solid particles in a density stratified fluid, *Phys. Fluids* **27**, 023302 (2015).
- [42] F. Blanchette and J. W. M. Bush, Particle concentration evolution and sedimentation-induced instabilities in a stably stratified environment, *Phys. Fluids* **17**, 073302 (2005).